Shape modeling technique KOALA validated by ESA Rosetta at (21) Lutetia

B. Carry[a], M. Kaasalainen[b], W. J. Merline[c], T. G. Müller[d], L. Jorda[e], J. D. Drummond[f], J. Berthier[g], L. O'Rourke[a], J. Ďurech[h], M. Küppers[a], A. Conrad[i], P. Tamblyn[c], C. Dumas[j], H. Sierks[k], and the OSIRIS Team[1]

[a]*European Space Astronomy Centre, ESA, P.O. Box 78, 28691 Villanueva de la Cañada, Madrid, Spain*
[b]*Tampere University of Technology, P.O. Box 553, 33101 Tampere, Finland*
[c]*Southwest Research Institute, 1050 Walnut St. #300, Boulder, CO 80302, USA*
[d]*Max-Planck-Institut für extraterrestrische Physik (MPE), Giessenbachstrasse, 85748 Garching, Germany*
[e]*Laboratoire d'Astrophysique de Marseille, Université de Provence, Marseille, France*
[f]*Starfire Optical Range, Directed Energy Directorate, Air Force Research Laboratory, Kirtland AFB, NM 87117-577, USA*
[g]*Institut de Mécanique Céleste et de Calcul des Éphémérides, Observatoire de Paris, UMR8028 CNRS, 77 av. Denfert-Rochereau 75014 Paris, France*
[h]*Astronomical Institute, Faculty of Mathematics and Physics, Charles University in Prague, V Holešovičkách 2, 18000 Prague, Czech Republic*
[i]*Max Planck Institute für Astronomy (MPA), Königstuhl 17, 69117 Heidelberg, Germany*
[j]*European Southern Observatory, Alonso de Córdova 3107, Vitacura, Casilla 19001, Santiago de Chile, Chile*
[k]*Max-Planck-Institut für Sonnensystemforschung (MPS), Max-Planck-Strasse 2, 37191 Katlenburg-Lindau, Germany*

arXiv:1112.5944v1 [astro-ph.EP] 27 Dec 2011

Abstract

We present here a comparison of our results from ground-based observations of asteroid (21) Lutetia with imaging data acquired during the flyby of the asteroid by the ESA Rosetta mission. This flyby provided a unique opportunity to evaluate and calibrate our method of determination of size, 3-D shape, and spin of an asteroid from ground-based observations. Knowledge of certain observable physical properties of small bodies (*e.g.*, size, spin, 3-D shape, and density) have far-reaching implications in furthering our understanding of these objects, such as composition, internal structure, and the effects of non-gravitational forces. We review the different observing techniques used to determine the above physical properties of asteroids and present our 3-D shape-modeling technique KOALA – Knitted Occultation, Adaptive-optics, and Lightcurve Analysis – which is based on multi-dataset inversion. We compare the results we obtained with KOALA, prior to the flyby, on asteroid (21) Lutetia with the high-spatial resolution images of the asteroid taken with the OSIRIS camera on-board the ESA Rosetta spacecraft, during its encounter with Lutetia on 2010 July 10. The spin axis determined with KOALA was found to be accurate to within two degrees, while the KOALA diameter determinations were within 2% of the Rosetta-derived values. The 3-D shape of the KOALA model is also confirmed by the spectacular visual agreement between both 3-D shape models (KOALA pre- and OSIRIS post-flyby). We found a typical deviation of only 2 km at local scales between the profiles from KOALA predictions and OSIRIS images, resulting in a volume uncertainty provided by KOALA better than 10%. Radiometric techniques for the interpretation of thermal infrared data also benefit greatly from the KOALA shape model: the absolute size and geometric albedo can be derived with high accuracy, and thermal properties, for example the thermal inertia, can be determined unambiguously. The corresponding Lutetia analysis leads to a geometric albedo of 0.19 ± 0.01 and a thermal inertia below $40\,\mathrm{J\,m^{-2}\,s^{-0.5}\,K^{-1}}$, both in excellent agreement with the Rosetta findings. We consider this to be a validation of the KOALA method. Because space exploration will remain limited to only a few objects, KOALA stands as a powerful technique to study a much larger set of small bodies using Earth-based observations.

Keywords:

1. Remote-sensing shape modeling

Perhaps the most striking observable of any asteroid is its shape. In 1993, spacecraft exploration revealed for the first time the stunning non-spherical shape of asteroid (951) Gaspra when NASA's Galileo spacecraft made the first of its two asteroid encounters, on its way to Jupiter. Asteroids had remained point-sources in the sky since the discovery of (1) Ceres in 1801 by Piazzi, almost two centuries before. Only the advent of space exploration and large Earth-based telescopes (*e.g.*, Arecibo and Goldstone radio telescopes, space-based-optical – HST, or ground-based near-IR, equipped with adaptive optics – Palomar, Lick, CFHT, Keck, ESO VLT, Gemini) allowed their apparent disks to be spatially resolved, and their irregular shapes to be imaged. The past decade has seen a revolution in our understanding of the physical properties (*e.g.*, size, 3-D shape, spin axis) of asteroids. This revolution has come about thanks to improved observing facilities and, of equal importance, from improved methods of analysis.

Determination of the physical properties for a statistically relevant set of asteroids has many implications for our under-

Email address: benoit.carry@esa.int (B. Carry)

[1]M. A'Hearn, F. Angrilli, C. Barbieri, A. Barucci, J.-L. Bertaux, G. Cremonese, V. Da Deppo, B. Davidsson, S. Debei, M. De Cecco, S. Fornasier, M. Fulle, O. Groussin, P. Gutiérrez, W.-H. Ip, S. Hviid, H. U. Keller, D. Koschny, J. Knollenberg, J. R Kramm, E. Kuehrt, P. Lamy, L. M. Lara, M. Lazzarin, J. J. López-Moreno, F. Marzari, H. Michalik, G. Naletto, H. Rickman, R. Rodrigo, L. Sabau, N. Thomas, K.-P. Wenzel

standing of these remnants of solar-system formation and, in turn, can be expected to improve our understanding of the history and evolution of the Solar System. For instance, the distribution of spin axes of the larger asteroids (diameter larger than ~100 km) on the celestial sphere is not expected to be isotropic. Numerical hydrocode simulations have predicted a slight excess in prograde rotators, due to the gas-pebble interaction in the protoplanetary disk (Johansen and Lacerda 2010). Similarly, the spin state of *small* asteroids (diameter not larger than few kilometers) is dominated by the non-gravitational YORP effect (Hanuš et al. 2011). Statistical knowledge of spin coordinates, how they are distributed within and among asteroid families of different ages, will provide strong constraints on the effectiveness of YORP (Slivan et al. 2003).

Reconstruction of the 3-D shape (including the size) is required to estimate the volume of an asteroid, which in turn is used to derive its density, possibly the property most fundamental to our understanding of an asteroid (Britt et al. 2002). Observations of the surface of an asteroid, such as colors, spectra, or phase effects, can provide clues to the surface composition of the asteroid. This may or may not be related to the bulk composition of the body (*e.g.*, Elkins-Tanton et al. 2011). Masses for asteroids can be determined from a spacecraft flyby, from the orbital motion of a natural moon, or even from the perturbations of asteroids on other bodies, such as Mars (Hilton 2002). In most cases, however, the uncertainty in the density is dominated by the uncertainty in the volume, rather than the uncertainty in the mass (Merline et al. 2002). Precise reconstruction of the 3-D shape is therefore of high importance for all asteroids for which a mass has been, or will be, estimated (*e.g.*, Hilton 2002; Mouret et al. 2007; Baer et al. 2011).

From the comparison of an asteroid's density with the densities of its most-likely constituents, we can constrain the macroporosity (large-scale voids) in its interior, probably produced by impacts over its history (Britt et al. 2002). These impacts could have partially disrupted the body, producing large-scale fractures, or even totally disrupted the body, with subsequent reaccumulation of the resulting fragments, leading to a "rubble-pile" structure.

Evidence of gigantic, but less than totally disruptive, impacts can be seen by high-resolution imaging and also inferred from our shape-modeling of asteroids. The huge impact craters evident in the images of C-type asteroid (253) Mathilde (Veverka et al. 1997) are thought to be about as large as could be sustainable by a body without disruption. There have been suggestions that these craters were created by compaction of low-density target material, rather than explosive ejection typical of hard-rock impacts (Housen et al. 1999). Already, our ground-based adaptive-optics imaging has shown what appear to be facets or depression-like features, similar to those seen on Mathilde, in some other large C-type asteroids (*e.g.*, (511) Davida in Conrad et al. 2007). Alternatively, some of our other images of C-type asteroids, such as (52) Europa, appear to bear no evidence of giant impacts (see Merline et al. 2011). Evaluation of the prevalence of such large impact events can give us insight into the size and frequency of these impact events over time, and thus into the history of the impacting population.

We summarize below the most common of the many observing techniques used to derive size, 3-D shape, and spin-vector coordinates and highlight some of their advantages and drawbacks. Then, in Section 2, we describe our KOALA multi-data shape-modeling algorithm. In Section 3, we present a comparison of the results produced by KOALA (from Earth-based observations) with those derived from the ESA Rosetta flyby of asteroid (21) Lutetia. In Section 4, we use our KOALA model in conjunction with mid-infrared data and a thermophysical model to derive the thermal properties of Lutetia and compare the results with those derived using thermal observations from the Rosetta spacecraft (Gulkis et al. 2011) and from the ground, making use of the shape model from the flyby (O'Rourke et al. 2011). We assess the accuracy of the KOALA shape-modeling method in Section 5.

1.1. Optical lightcurve

Historically, spin properties and triaxial-ellipsoid shapes have been studied largely through observations of rotationally induced variability in disk-integrated brightness (lightcurves). Indeed, the object's shape, its rotational state (period and spin-vector coordinates), and the scattering properties of its surface can be determined from the analysis of its lightcurves over time (as the viewing/illumination geometry changes).

For about a decade, starting with the lightcurve inversion algorithm presented by Kaasalainen and Torppa (2001) and Kaasalainen et al. (2001), lightcurves also have been used extensively to derive 3-D shape models of asteroids (see the examples for asteroids Gaspra and Šteins in Fig. 1). The 3-D shape models and spin properties of more than 200 asteroids already have been derived (these are accessible from DAMIT [2], see Ďurech et al. 2010). These shape models are, however, limited to dimensionless, *convex* shapes, with limited spatial resolution. Recently, Ďurech et al. (2011) have shown that the size of these models can be set by using other types of input data (*e.g.*, stellar occultation profiles, see Sect. 1.2). The intrinsic *convex* nature of the models precludes accurate determination of the volume, and hence density, of the objects, however.

Because lightcurve observations require neither large telescope aperture nor specialized instrumentation, they are, and will remain, a major source of information on small bodies. Thousands of lightcurves, for hundreds of asteroids [3], have been accumulated during the last half century. Amateur astronomers contribute significantly to this ever-growing database of lightcurves [4] (*e.g.*, Behrend et al. 2006; Ďurech et al. 2007).

Sparse photometry (*i.e.*, when the typical separation between measurements is larger than the rotation period, as opposed to historical lightcurves, which are dense in time) can also be used

[2] DAMIT: http://astro.troja.mff.cuni.cz/projects/asteroids3D/web.php

[3] *e.g.*, the Asteroid Photometry Catalogue (APC) or the Asteroid Lightcurve Database (LCDB, Warner et al. 2009) list more than 6000 lightcurves for about 700 asteroids:
APC: http://asteroid.astro.helsinki.fi/apc
LCDB: http://www.minorplanet.info/lightcurvedatabase.html

[4] *e.g.*, about 2300 lightcurves for more than 1700 asteroids have been acquired by the CdR group: http://obswww.unige.ch/~behrend/page_cou.html

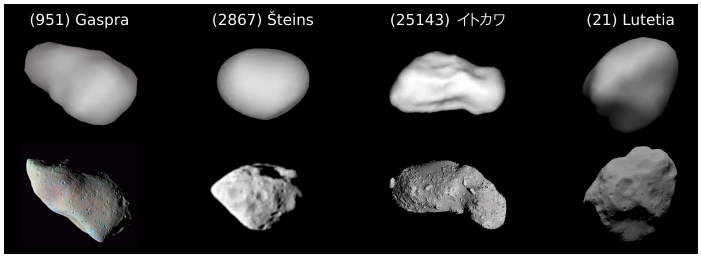

Figure 1: Comparison of four shape models, derived using ground-based observations, with high-spatial-resolution images obtained *in situ* by spacecraft (left-to-right): (951) Gaspra lightcurve inversion model from Kaasalainen et al. (2002a), image from NASA Galileo; (2867) Šteins lightcurve inversion model from Lamy et al. (2008a,b), image from ESA Rosetta; (25143) Itokawa radar delay-Doppler model from Ostro et al. (2005), image from JAXA Hayabusa; and (21) Lutetia KOALA model from Carry et al. (2010b) and Drummond et al. (2010), image from ESA Rosetta.

to reconstruct 3-D models (see Kaasalainen 2004). Hanuš et al. (2011) have used a combination of sparse photometry, together with dense lightcurves, to derive about 100 new shape models, using measurements extracted from large all-sky surveys (such as USNO, Catalina, Siding Spring, and Hipparcos). Knowledge of the absolute photometry (as opposed to relative photometric measurements, as in a dense lightcurve) is, however, required to make these sparse measurements useful to 3-D shape modeling (see Hanuš et al. 2011, for a detailed discussion). From the upcoming PanSTARRS and Gaia surveys we can expect hundreds of thousands of objects to be modeled using this method (Ďurech et al. 2005).

1.2. Stellar occultation

Occultations occur when a solar-system object passes between a star and Earth, causing the asteroid's shadow to cross some portion of Earth as a track. Because the star is very far relative to the Earth-asteroid separation, the shadow cast by the asteroid is effectively parallel. Thus, the width of the shadow track (perpendicular to the track) gives the maximum width of the asteroid in the cross-track direction. It is usually not possible to get a high density of observers stationed across the track, and thus this dimension may not be so well established. But along the track, the size of the asteroid, as an along-track chord on the asteroid, corresponding to the position of the observer within the shadow, is given by the length of time of the blink-out event. With many observers, many along-track events can be recorded and the blink-out intervals are converted to chord lengths at the asteroid by using the asteroid's known speed (see Millis and Dunham 1989, for a review).

One advantage of stellar occultations is that very small minor planets can be probed (provided one accounts properly for diffraction effects). Even stellar occultations by small trans-Neptunian objects (TNOs) of a few kilometers diameter can be recorded (see Roques et al. 2009). Finally, stellar occultations provide a powerful means for studying thin atmospheres and/or exospheres (*e.g.*, Sicardy et al. 2003).

In theory, three occultation events (each recorded by enough observers to secure a unique apparent-ellipse to be fit on the chords) provide enough constraints to determine the triaxial dimensions (ellipsoid) and spin-vector coordinates of an asteroid (Drummond and Cocke 1989; Dunham et al. 1990). The number of chords that result from an event will often be larger with brighter occulted stars. This is because many more observers can be fielded if the required telescope aperture is modest. In practice, however, occultations of bright stars by any given asteroid occur rather infrequently. This difficulty in obtaining sufficient chords, plus the noise level often encountered (especially the systematic errors coming from imperfect knowledge of asteroid and star astrometry, combined with observer timing errors), strongly limit our ability to construct 3-D shape models and derive spin properties from occultations alone. Nevertheless, stellar occultations are an efficient way to provide additional size/shape information, particularly for shape models that otherwise lack a scale, such as those from lightcurves alone (see 1.1 and Ďurech et al. 2011).

With the availability of low-cost GPS positioning equipment and CCD cameras (the majority of measurements are made by amateur astronomers), the accuracy of occultation timings has improved greatly over the last decade. From this improved precision, together with the refinement of the orbits of small bodies expected to result from Gaia/PanSTARRS (allowing an extremely precise prediction of the occultation track on Earth, see Tanga and Delbo 2007), we can expect that stellar occultations will become ever more useful in the determination of certain physical properties of asteroids, especially for objects having small angular diameters.

1.3. Thermal radiometry

The amount of thermal emission from an asteroid is mainly a function of its physical diameter and surface albedo, and, to a lesser extent, the physical properties of its surface (*e.g.*, thermal inertia, roughness). Main-belt asteroids are among the brightest sources in the sky in the mid-infrared (5–20 microns), so infrared satellites (IRAS, ISO, AKARI, Spitzer, Herschel, WISE) have been able to acquire observations of a vast number of these objects (see Mainzer et al. 2011, for instance).

Estimates for size and albedo are model-dependent, however, and several thermal models co-exist, from the simple Standard Thermal Model (STM) of non-rotating spheres of Lebofsky et al. (1986) to the detailed Thermophysical Model (TPM) of Lagerros (1996, 1997), having a complete description of 3-D shape and surface properties. Unfortunately, the systematic uncertainties involved when applying those models (resulting from their respective assumptions and approximations) are not always properly taken into account in estimating error bars, and results often differ from one determination to another by more than the quoted uncertainties (see Table 3 in Delbo and Tanga 2009, illustrating the issue). For instance, it now seems that the database of 2 228 diameters (Tedesco et al. 2002) estimated using the overly simple STM with IRAS data may be biased by a few percents (see the re-analysis of IRAS data by Ryan and Woodward 2010).

The radiometric technique to derive sizes and albedos from thermal infrared data benefits greatly from the availability of 3-D shape models. For example, the absolute size of

(25143) Itokawa derived by Müller et al. (2005), based on a 3-D shape model implementation in a TPM code, agreed to within 2% of the final in-situ result from the Hayabusa mission (Fujiwara et al. 2006). In general, mid-infrared observations are highly valuable for scaling dimensionless shape models (similar to the situation with stellar occultations, as mentioned in Sect. 1.2) and mid-infrared data are available for several thousand asteroids. These data even allow determination of the most likely spin-axis solutions in cases where lightcurve inversion techniques lead to more than one possible shape and spin-axis solution (see, *e.g.*, Müller et al. 2011, for a recent example). In cases where the shape-model already comes with size information (or alternatively, if many thermal observations are available for a given target), it is possible to derive the thermal inertia, indicative of the surface characteristics: *e.g.*, bare rock, ice, boulders, dust regolith (see, for instance Müller et al. 2005; Delbo et al. 2007, among many others).

In some particular cases of extensively observed asteroids, the thermal radiometry can also provide hints on the 3-D shape, through the measure of the apparent projected cross-section of the asteroid on the plane of the sky at each epoch. By comparing the predicted with observed thermal fluxes of Lutetia under many geometries, O'Rourke et al. (2011) have shown that adding a hill/plateau, whose size remains within the quoted 3-D shape uncertainty, could explain the discrepancies observed for a certain observing geometry.

1.4. Radar delay-Doppler echoes

Radar observations consist in transmitting a radio signal toward the target and recording the echo. The distribution of the echo power in delay time and Doppler frequency is related to the spin state and 3-D shape of the target (see the reviews by Ostro 1989; Ostro et al. 2002). The time and frequency precision currently achievable (Arecibo, Goldstone) allow the study of very small objects, the main limit of radar observations being the distance of the target (echo power scales inversely with distance to the fourth power). This is why most radar studies have concentrated on Near-Earth Objects (NEOs), while dedicated observations of Main-Belt Asteroids (MBAs) have been more limited (see Ostro et al. 2002).

The difficulty in constructing 3-D shapes from a series of delay-Doppler "*images*" is due to the absence of a direct, one-to-one, link between each region of the surface with a pixel in delay-Doppler space. Indeed, all points situated at the same range from the observer, and moving at the same radial velocity (possibly spread over the apparent disk) will contribute to a single delay-Doppler pixel. So delay-Doppler images are many-to-one maps of the shape as highlighted by Ostro et al. (2002): there is no *a priori* way to determine how many regions will contribute to a single pixel, which strongly contrasts with the one-to-one mapping ("WYSIWYG") achieved in disk-resolved imaging.

Radar echoes remain, however, the best way to determine the physical properties of NEOs (*e.g.*, the very small NEO Itokawa in Fig.1). For instance, the possible migration of the regolith at the surface of a fast-rotating asteroid triggered by YORP spin-up (Walsh et al. 2008) was suggested by the detailed 3-D shape of the NEO (66391) 1999 KW_4 (Ostro et al. 2006).

1.5. Disk-resolved imaging

Since the 1990s, with the advent of the Hubble Space Telescope and large ground-based telescopes equipped with adaptive optics (AO: Lick, CFHT, Keck, ESO VLT, Gemini), we have access to the angular resolution required to resolve the apparent disk of asteroids (*e.g.*, Saint-Pé et al. 1993a,b; Drummond et al. 1998; Parker et al. 2002, 2006).

From a time-series of disk-resolved images, spin-vector coordinates can be derived (using previous knowledge of the rotation period) by analyzing the changes in the apparent shape of the asteroid profile (see for instance Thomas et al. 1997b; Drummond and Christou 2008), or by following the apparent path taken by an albedo patch on the surface during the rotation (*e.g.*, Thomas et al. 2005; Carry et al. 2008). Triaxial shapes (ellipsoids) can also be derived (see Drummond et al. 2009; Schmidt et al. 2009, for instance), and topography (such as the presence of facets or craters) studied from profile deviations to the ellipsoid (*e.g.*, Thomas et al. 1997a; Conrad et al. 2007). With sufficient spatial resolution, imaging of the asteroid disk can allow construction of albedo maps of the surface, allowing the study of composition heterogeneity or localized space weathering effects (*e.g.*, Binzel et al. 1997; Li et al. 2006, 2010; Carry et al. 2008, 2010a). In the case of asteroids visited by spacecraft, high spatial-resolution and precise photometry can be used to derive precise shape and digital terrain models by using stereophotoclinometric techniques (see examples in Gaskell et al. 2008).

The size and 3-D shape resulting from disk-resolved images are of great value, being obtained in a direct manner (as compared to an indirect determination of the shape from lightcurve inversion, for instance). The best angular resolution [5] of current Earth-based telescopes is about 0.04″. Due to systematics, however, we have found that our ability to accurately measure sizes degrades rapidly below about 0.10″, based on simulations and observations of the moons of Saturn and other objects (Carry 2009; Drummond et al. 2009). The sample of asteroids observable (*i.e.*, having angular sizes that get above about 0.10″) is therefore limited to about 200 (over a given 10-year span).

1.6. Interferometry

Apart from building larger telescopes, one efficient way to improve the angular resolution is to combine light beams from separated telescopes and to observe the resulting interference (fringes). In such a mode, each telescope aperture plays the role of a sample aperture within a virtual telescope whose extent is the largest distance between the two telescopes (the spatial resolution Θ is still given by the equation in footnote 5, except that

[5] limited by the diffraction, which acts as a low-pass filter with a cutoff frequency approximated by $\Theta = \lambda/\mathcal{D}$ (radian), λ being the wavelength and $\mathcal{D}$ the diameter of the telescope aperture.

$\mathcal{D}$ is now the *distance* between the apertures). For instance, with telescopes separated by about 80 m, the VLTI provides an order-of-magnitude improvement in angular resolution over a single telescope of the VLT (8 m aperture).

This improvement in the resolution, however, occurs at the price of a loss in complete spatial information, because the virtual aperture is under-sampled. The very high angular-resolution is limited, at a given instant, to a single line on the plane of the sky, which is given by the baseline linking the two apertures. Along that baseline, the signal is directly related to the Fourier transform of the flux distribution on the plane of the sky. To expand the coverage in the spatial-frequency domain, and thus to allow the construction of 2-D images of the target, one must increase the number of projected baselines. This is commonly achieved by either adding multiple physical baselines (*i.e.*, adding more telescopes) and/or by making observations throughout the night, as the Earth's rotation causes a progression of the position angle of the baseline on the sky. However, because asteroids typically complete their rotation in only a few hours, the method using multiple telescopes is more effective at providing higher spatial sampling. Below we describe another promising technique to effectively increase the number of baselines, by using a Fizeau design.

For objects with no a priori information, the overall dimensions and spin properties can be determined under the assumption that the shape is well-described by a triaxial ellispoid (Li et al. 2011). For example, the two orthogonal directions of the Fine Guidance Sensor (FGS) on-board HST have been used to study binarity and measure the size of several MBAs (Tanga et al. 2001; Hestroffer et al. 2002; Tanga et al. 2003). The fringes of interference, however, also contain information on the apparent shape, and can be used in combination with other data to derive 3-D shape models. For instance, Kaasalainen and Lamberg (2006) used FGS data in combination with optical lightcurves to refine the 3-D shape model of (15) Eunomia from Kaasalainen et al. (2002b).

Interferometry in the mid-infrared has been used recently also, with promising results. In this wavelength regime, the signal is linked to the distribution of temperature (*i.e.*, *emitted* light) on the surface of the target (as opposed to the reflected light seen at visible wavelengths). Delbo et al. (2006) and Delbo et al. (2009) have combined thermal infrared TPM models (see Sect. 1.3) with interferometry, allowing the size of 3-D shape models to be set (similar to stellar occultation and thermal-infrared-only, see Sections 1.2 and 1.3 and Matter et al. 2011).

The current limitation of interferometry is set by the sensitivity of available facilities and is driven largely by the integration time, which is usually short. Because the light beams from the two apertures traverse different paths in the atmosphere, their wavefronts encounter different turbulence-dominated perturbations, leading to a shift in their phase. Delay lines are used to "slow down" one beam with respect to the other, and to match their phase. The technical difficulties in maintaining coherence in this process limits the integration time to few hundredths or thousandths of a second. A new generation of instruments (like PRIMA at VLT) with fringe-tracking systems will overcome this limitation in the near future, allowing fainter sources to be targeted.

An interesting compromise between co-axial interferometers and traditional, filled aperture, telescopes can be found in Fizeau-type instruments such as LINC-NIRVANA, being built for the Large Binocular Telescope (LBT, see Hill et al. 2010), in which improved coverage of the spatial-frequency plane (commonly called uv-plane, with u and v standing for the two orthogonal unit directions) can be achieved in less telescope time. This design (Fizeau *vs.* pupil-plane interferometer like the VLTI) allows instantaneous filling of the uv-plane up to the frequency set by the 8 m apertures (Fizeau interferometers are true imaging devices and produce direct images of the plane of the sky), with an additional filling along one dimension up to the frequencies corresponding to the maximal baseline (22.7 m for LBT). Two or three epochs, with different position angles of the baseline on the plane of the sky, will be enough to fill the uv-plane up to the maximal extent of the telescope (achievable for transiting asteroids, especially with high elevation, when the position angle evolves quickly). For this purpose, therefore, the LBT is equivalent to a 22.7 m telescope with a mask, corresponding to the configuration of component apertures, placed in the entrance pupil.

The opening of interferometric studies to longer wavelengths also has great potential, with the use of millimeter and sub-millimeter arrays, where there are fewer technological limitations than in the optical range. Future facilities such as ALMA, with 50 antennas (translating into 1 225 baselines *vs.* only 2 baselines for MIDI at the VLTI, see Delbo et al. 2009), will allow dense spatial coverage, together with an angular resolution of few milli-arcseconds. Simulations have shown that several hundreds of MBAs and TNOs will be observable with ALMA (see Busch 2009; Moullet et al. 2011). Interferometry at thermal wavelengths (mid-infrared to millimeter), in combination with other techniques (*e.g.*, lightcurves, see Sect. 1.1), will thus allow the derivation of 3-D shape models, together with thermal properties, for many asteroids of small apparent diameter.

2. The KOALA algorithm

With advantages and drawbacks of each observing technique in mind, we have developped a multi-data inversion algorithm: Knitted Occultation, Adaptive-optics, and Lightcurve Analysis (KOALA), that makes simultaneous use of data from three distinct observation types[6] to determine the physical properties of asteroids (Carry et al. 2010a; Kaasalainen 2011). KOALA takes advantage of the direct measure of the apparent size and shape of asteroids on the plane of the sky provided by the timings of stellar occultations and disk-resolved images, and of the indirect constraints on spin and 3-D shape given by lightcurves. We quickly summarize below how the inversion works (see Kaasalainen 2011, for a comprehensive description of the algorithm).

[6] We categorize dense (*i.e.*, lightcurves) and sparse photometry together to form a single data type.

KOALA is a step-iterative minimization algorithm, solving for the spin parameters (spin-vector coordinates λ, β, and sidereal period $\mathcal{P}$), 3-D shape (given by a set of $\mathcal{N}$ coefficients of spherical harmonics, including the overall size), phase function (defined as a three-parameter model, see Kaasalainen and Torppa 2001; Kaasalainen et al. 2001), and scattering law (generally taken as a combination of the Lommel-Seeliger and Lambert diffusion laws, following Kaasalainen and Torppa 2001, although other models such as Hapke can be used).

From a set of estimated parameters (determined from lightcurve-only inversion or analysis of the disk-resolved images, for instance), a trial solution is created, with associated synthetic data sets (*i.e.*, simulated lightcurves, disk-resolved images, and occultation profiles). KOALA then follows a Levenberg-Marquardt minimization scheme to determine the set of parameters that best fit all the data sets simultaneously, by comparing at each step the synthetic data with real measurements. The iteration stops when the residuals between the simulated and measured data sets reach an acceptable level (*i.e.*, the level of the intrinsic noise of the measurements).

As a safeguard, the resolution (*i.e.*, $\mathcal{N}$) is set to the lowest possible value for which a fit to the data can be achieved. We also introduced several regularizations: (a) a non-convexity ("smoothness") term, that avoids spurious features (unrealistic topography) at small scales, unconstrained by the data; and (b) an inertia tensor regularization for principal-axis rotators, that forces the asteroid spin-axis to remain aligned, within a few degrees, with the largest moment of inertia. The relative weights of the different data types and also of the regularizations are determined using the maximum compatibility estimate of Kaasalainen (2011), instead of being subjective.

3. KOALA and Rosetta-flyby shape model

On 2010 July 10, the ESA Rosetta spacecraft made a close flyby of the main-belt asteroid (21) Lutetia. In support of the mission, we had combined optical lightcurves with disk-resolved images, from ground-based AO. We produced a full 3-D shape model of Lutetia, using KOALA, months before the encounter (see Drummond et al. 2010; Carry et al. 2010b, and Fig. 1). This flyby provided a rare opportunity to test and calibrate KOALA with close-up spacecraft imaging.

The closest approach (CA) occurred at 3 170 km from the asteroid at a relative speed of 15 km/s. The Narrow Angle Camera (NAC) of the OSIRIS instrument on-board Rosetta (Keller et al. 2007) returned a total of 202 images during the flyby, which spanned about 9 h. The NAC image scale ranged from 5 000 to 60 m/pix, reaching its minimum value at CA. These very high spatial-resolution images have been used to produce detailed 3-D shape models of Lutetia, using stereophotoclinometry (Sierks et al. 2011), and stereophotogrammetry (Preusker et al. 2011). We only consider here the model from Sierks et al. (2011), these two models being similar enough at the medium-to-large scale for our purpose.

Lutetia's spin axis is tilted such that its pole is nearly in its orbital plane (obliquity of 96°, see Carry et al. 2010b; Sierks et al. 2011). At the time of the Rosetta flyby, the southern hemisphere was in seasonal shadow, and observations at optical/near-infrared wavelengths were not possible south of -40° latitude. The detailed 3-D shape model derived from flyby images by stereophotoclinometry (Sierks et al. 2011) therefore does not cover a large fraction of the asteroid's southern hemisphere (see Fig. 2), the southernmost portion of the shape model being determined using the KOALA algorithm together with the ground-based data from Carry et al. (2010b). Almost all of the AO images that entered into the KOALA solution, even though from multiple epochs, were taken looking at either high southerly or high northerly sub-Earth latitudes (see Carry et al. 2010b; Drummond et al. 2010). For both the ground-based KOALA and the flyby analyses, therefore, the shortest (c) dimension (Table 1) is not well constrained and represents the largest contribution to the uncertainty in the volume estimates.

	Diameters (km)				Spin axis (°)			
	d	a	b	c	λ	β	$\pm$	σ
KOALA	105	124±5	101±4	93±13	52	-6	± 5	
OSIRIS	98	121±1	101±1	75±13	52.2	-7.8	± 0.4	

Table 1: Comparison of the dimensions and spin-vector coordinates of (21) Lutetia derived from OSIRIS images during the ESA Rosetta flyby (Sierks et al. 2011) with those derived by KOALA (Drummond et al. 2010; Carry et al. 2010b) prior to the flyby. Volume-equivalent diameter (d) and triaxial diameters ($a > b > c$) are reported in km, and spin-vector coordinates in degree (longitude λ, latitude β in the ECJ2000 reference frame, with σ the angular radius of the uncertainty circle).

We first present (Section 3.1) an overall comparison of our size and spin estimates (based on ground-based techniques) with those derived from the analysis of the very high spatial-resolution images acquired by OSIRIS (Sierks et al. 2011). We then directly compare the predicted shape profiles, based on KOALA, with those images (Section 3.2), seeking to calibrate our method.

3.1. Overall comparison

In this section, we present a comparison of the spin-vector coordinates and dimensions derived from the flyby with the pre-flyby values from KOALA (Table 1). Because southerly latitudes were not visible during the flyby and the c-dimension in the OSIRIS model comes from a combination of OSIRIS imaging and KOALA model information, the OSIRIS c-dimension is not wholly independent. But the spin-vector coordinates and equatorial dimensions (a, b) from the OSIRIS analysis can be used as "ground-truth" to calibrate our KOALA method.

First, the spin-vector coordinates agree to within two degrees [7], well inside the 5° uncertainty quoted for KOALA Then, equatorial dimensions (a and b) are within 3 km of the flyby estimates, again well within the uncertainties reported for each dimension using KOALA. The larger difference between the estimates of the short (c) axis results from the expansion of the

[7] the coordinates obtained with KOALA are 1.2° and 1.8° from the spin-vector solutions derived by F. Preusker ($\lambda = 52.6°$, $\beta = -7.1°$, pers. communication) and by Sierks et al. (2011) respectively, using the OSIRIS images.

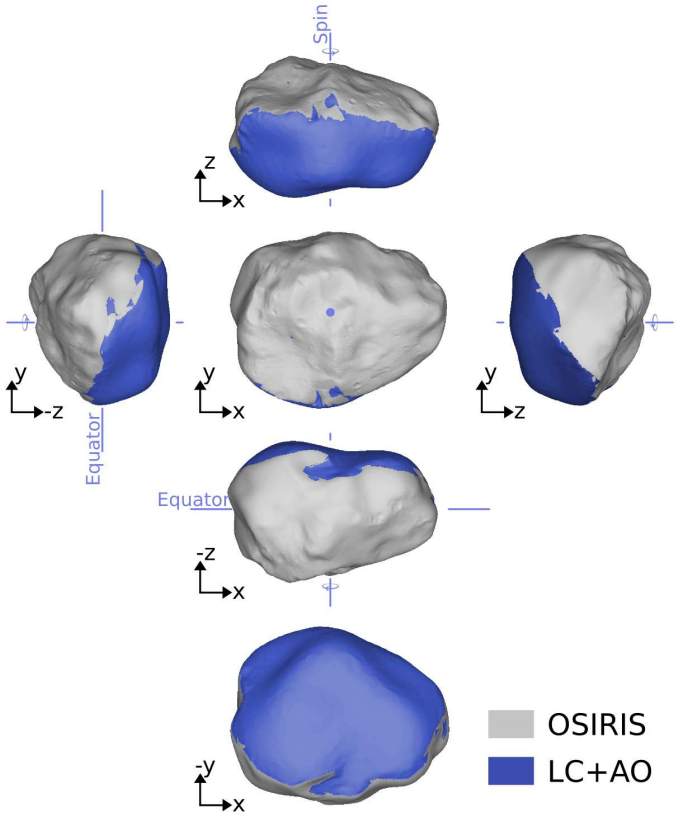

Figure 2: Lutetia 3-D shape model from Sierks et al. (2011), displayed in a net layout. Regions imaged by OSIRIS are displayed in gray. The part of the shape model that is based on ground-based data only (lightcurves and images: LC+AO) is plotted in blue.

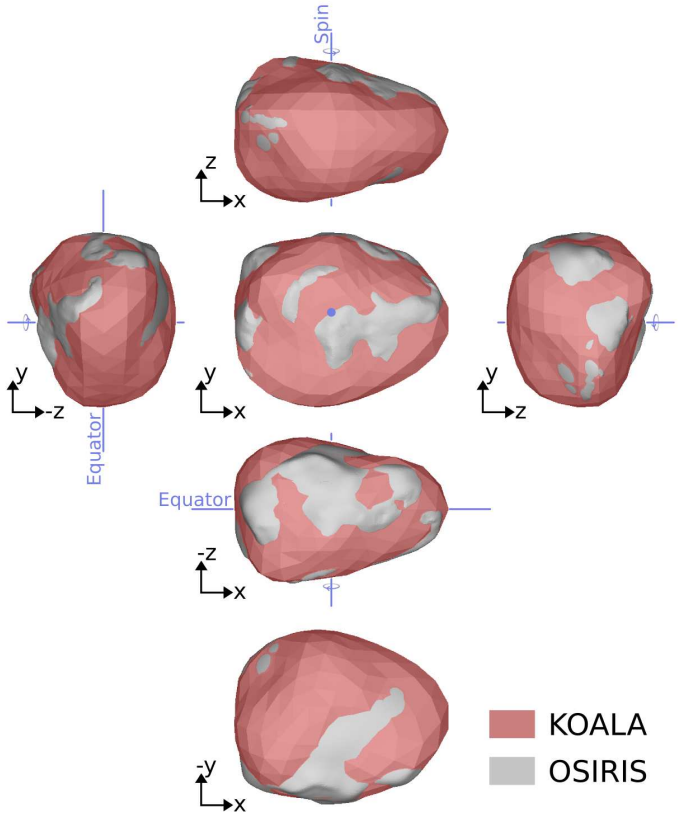

Figure 3: Similar plot as Fig. 2, showing the agreement between the pre-flyby KOALA (reddish, Carry et al. 2010b) and post-flyby (grayish, Sierks et al. 2011) shape models of (21) Lutetia. The radii of the KOALA model are larger in red regions, and those of the OSIRIS model in gray regions. The amalgam of gray and red colors illustrates the spectacular agreement between the results from the Rosetta flyby and our KOALA model obtained before the flyby. The dominance of red hues, however, highlights the relativly lower sensitivity to concavities of the KOALA model with respect to the OSIRIS 3-D shape. Shown in this comparison is the original KOALA model of Carry et al. (2010b), with a c-dimension of 80 km (overall size $124 \times 101 \times 80$ km), rather than the modified KOALA ("hybrid") estimate of Drummond et al. (2010), having a c-dimension of 93 km and shown in Table 1. This is a more realistic comparison for the figure because much of the southern hemisphere of the OSIRIS model (Fig. 2) is based on the data that entered into the original KOALA model.

KOALA c dimension from its original 80 km to 93 km, based on the analysis by Drummond et al. (2010). Indeed, the best-fit solution for all the AO images (including an additional observation taken with a more equatorial geometry, presented by Drummond et al. (2010) and not used by Carry et al. (2010b) owing to calibration issues, see Carry et al. for details) pointed toward a larger c dimension (supported by independent considerations on the amplitude of lightcurves by Belskaya et al. 2010). The volume-equivalent diameter is, therefore, larger (105 *vs.* 98 km) for the KOALA model than for the flyby-derived model by Sierks et al. (2011). Disk-resolved images of Lutetia taken with low sub-observer latitudes are required to confirm its c dimension, and to set tighter constraints on its volume.

The depth of large-scale concavities was slightly underestimated by KOALA (Fig. 3); estimating the depth of a concavity from profiles only is problematical because the concavity is hidden behind its rim. With stereophotoclinometry, is is possible to sense depths. In addition, while KOALA is sensitive to large-scale concavities, the necessarily limited resolution when imaging from a distance of 200 million km means that it is less sensitive to small-to-medium-scale concavities. We evaluated the influence of craters on the volume of Lutetia. For that, we used the crater size distribution measured by Marchi et al. (2011), and estimated their volume as that of a spherical cap ($V_{\rm crat}$), using the average depth-to-diameter ratio measured by Vincent et al. (2011):

$$V_{\rm crat} = \frac{\pi}{6} d \left(\frac{3}{4} D^2 + d^2 \right) \quad (1)$$

where d is the depth of the crater and D its diameter. We present in Fig. 4 the cumulative distribution of the volume encompassed by craters, counted on four geomorphological units (see Thomas et al. 2011, , for a detailed definition of the units), against their diameter. The vast majority of the volume is due to the handful of craters with diameters between 10 and 20 km. The total influence of these craters on the volume of Lutetia is $0.6 \pm 0.1\%$, *i.e.*, the volume of Lutetia would be 0.6% larger if these craters were not included in the 3-D shape model. Extrapolating this value, by considering the area covered by these

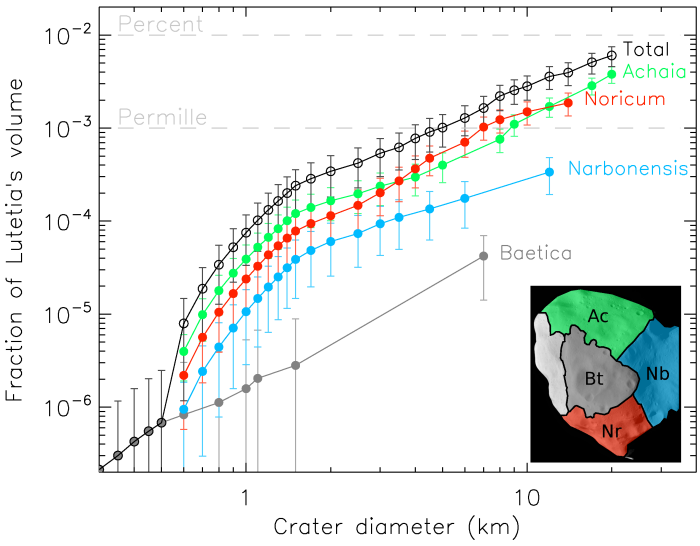

Figure 4: Cumulative distribution of the volume encompassed by craters as function of their diameter, for four geomorphological units of Lutetia: Achaia (Ac), Baetica (Bt), Narbonensis (Nb), and Noricum (Nr) (see the insert, adapted from Fig. 1 by Sierks et al. (2011), and also Thomas et al. (2011) for the definition of these units).

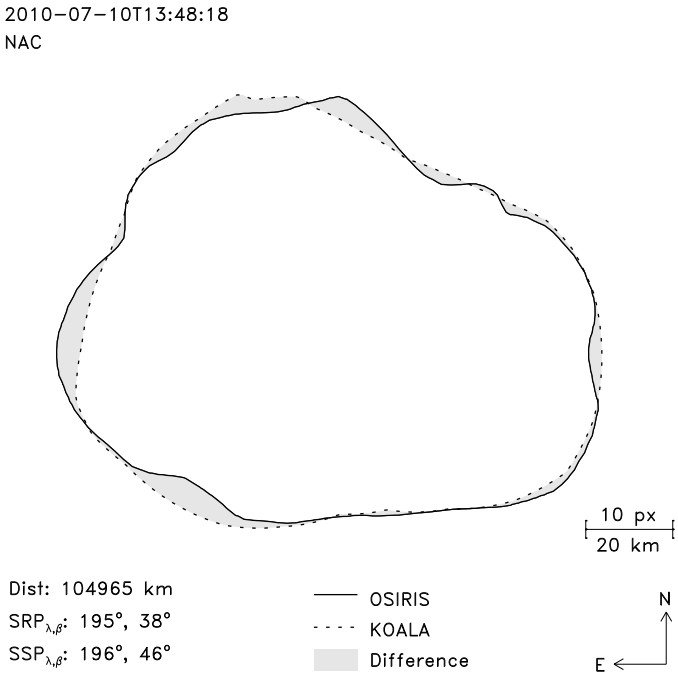

Figure 5: Example of a profile comparison, as measured on the OSIRIS NAC detector plane (solid line) and simulated from the KOALA model (dotted line), taken at 13:48:18 UT (CA - 1h57m). The light gray area represents the difference in projected area on the plane of the sky between the prediction and the observation. We report the Rosetta-Lutetia distance, the coordinates of the sub-Rosetta point (SRP) and subsolar point (SSP), and a scale for angular (OSIRIS NAC pixels) and physical dimension.

unit to the whole surface of Lutetia, make the total[8] influence of craters to be $2.4 \pm 0.6\%$.

Proper modeling of the craters in the 3-D shape model (from high-resolution flyby images, Sierks et al. 2011) is therefore crucial, given the level of accuracy reached elsewhere on the surface. For Earth-based observations, however, this will remain a minor source of uncertainty: depending on the methods, the volume accuracy ranges from few percent to few tens of percent (see Sect. 1). We discuss in the next section (3.2) the influence of these craters on the volume accuracy that can be reached using KOALA.

3.2. Detailed analysis

We push further the calibration of the KOALA method by comparing comprehensively the KOALA shape model predictions with the very high-spatial-resolution images provided by OSIRIS NAC. In the absence of a complete 3-D shape model, based on an entirely independent data set, it is difficult to fully calibrate the volume estimate provided by KOALA. For each OSIRIS image, we extracted the profile of the apparent disk of Lutetia, composed of its limb and its terminator. We produced synthetic views of the KOALA shape model under the same geometry (*i.e.*, as seen from Rosetta, see Fig. 5): phase angle, subsolar point (SSP) and sub-Rosetta point (SRP) coordinates, using the Miriade[9] VO ephemeris generator[10].

We estimate the fit of KOALA predictions to OSIRIS data by computing the difference between the projected areas on the plane of the sky. The relative accuracy of the volume determination ($\delta V/V$) can then be determined as follows:

$$\frac{\delta V}{V} = \frac{3}{2}\frac{\mathcal{A}_O - \mathcal{A}_K}{\mathcal{A}_O} \qquad (2)$$

where $\mathcal{A}_K$ and $\mathcal{A}_O$ are the areas of the KOALA prediction and on OSIRIS frame, respectively. Negative and positive δV respectively indicate an overestimate or underestimate of the volume by the KOALA model. We discarded from the current analysis the images taken close to CA, which have substantial phase angle (above 10°), where local topography (*e.g.*, crater rims) produce large projected shadows, increasing the uncertainty in the prediction of the terminator position on the surface of Lutetia.

From this detailed analysis, we confirm the results from the overall comparison presented in Section 3.1: the volume was slightly overestimated with KOALA, relative to the results derived from the flyby. But, as visible in Fig. 6, the difference between the KOALA predictions and the OSIRIS images is almost constant, at about -5%, for all images taken with phase angle smaller than ~10°. The largest deviations, still within the uncertainty reported using KOALA, are found for sub-Rosetta latitudes lower than about 40°, *i.e.*, for geometries that had not been observed from Earth with AO. Owing to the restricted geometries of ground-based AO imaging observations to date (always close to "pole-on", see Drummond et al. (2010) and Carry et al. (2010b)), the differences between KOALA predic-

[8] Because the shape of the southern hemisphere is poorly constrained, and the number of craters there unknown, this extrapolated value is only a rough estimate.

[9] http://vo.imcce.fr/webservices/miriade/

[10] we used Rosetta flight kernel ORHR_____00122.BSP

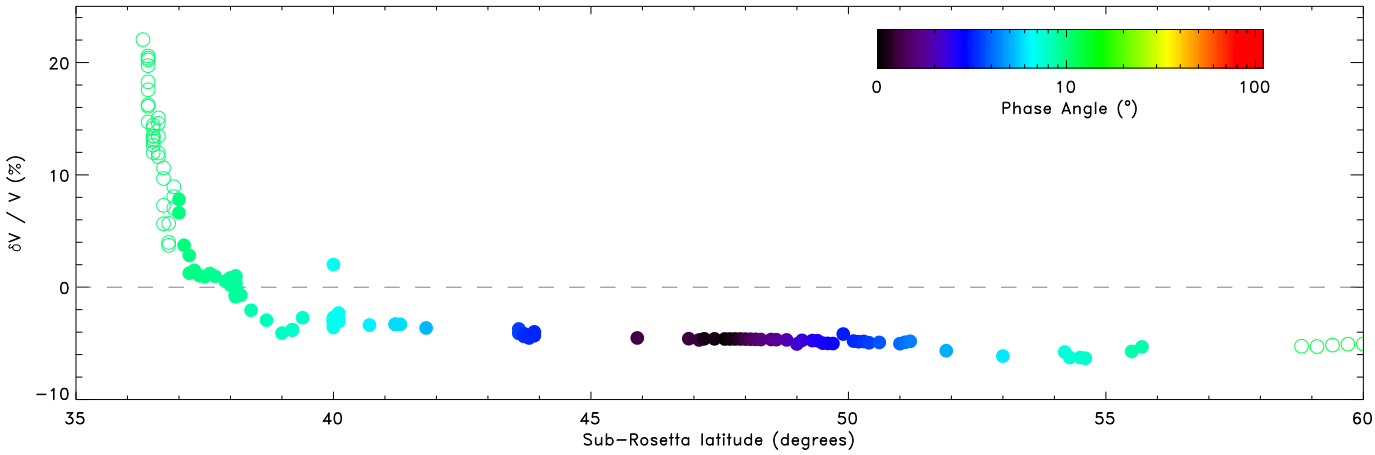

Figure 6: Difference in volume estimated (Eq. 2) from the difference in projected area between the profiles of Lutetia extracted from the OSIRIS images and the prediction from the KOALA model (Carry et al. 2010b). The symbols are color-coded as a function of the phase angle. Filled symbols correspond to images where the phase angle was smaller than 10°.

tions and OSIRIS frames may be related to two distinct factors: one "inherent" to KOALA (which is the one we seek to evaluate), and another related to the observing geometry. Unfortunately, there is no easy way to distinguish between these two effects. We thus estimate that the inherent uncertainty in the KOALA volume is about 5% (Fig. 6). This uncertainty can increase, however, due to unfavorable observing geometries, such as we have for the present case of Lutetia.

In addition to calibrating the volume estimate, we assess the accuracy of the KOALA 3-D shape determination. From the direct comparison of both models (pre- and post-flyby, in Fig. 3), we can already qualitatively assert that KOALA allows accurate 3-D shape determination. However, many different shapes can result in similar volume, and also in similar overall triaxial-ellipsoid dimensions (which are accurate to a couple of km, see Section 3.1). We therefore apply the following criterion (δR, see Eq. 3) to estimate the *local* deviation of the KOALA model to the real shape of Lutetia, and therefore calibrate quantitatively the KOALA 3-D shape determination:

$$\delta R = \frac{1}{N} \sum_{i}^{N} \frac{(O_i - \mathcal{K}_i)^2}{O_i} \qquad (3)$$

where O_i and $\mathcal{K}_i$, respectively, are the OSIRIS and KOALA profile radii of the ith point (out of N describing the OSIRIS profile), measured from an arbitrary center.

We present in Fig. 7 the estimate of the local deviation of the KOALA predictions to the apparent shape of Lutetia measured on the OSIRIS NAC images, as a function of the time relative to CA. The deviations are limited to about 4 km at maximum, and are about 2 km on average (confirmed by the independent analysis of Preusker et al. 2011). The typical accuracy in the elevation of each vertex is therefore close to 2 km. This is consistent with the overall comparison presented in Section 3.1, but we show here that not only the overall sizes are accurate to about 2 km, but that this accuracy is maintained at local scales.

The *apparent* absence of craters in the KOALA model[11] (compared to 3-D shape models derived from flyby, *e.g.*, Sierks et al. 2011; Preusker et al. 2011) has therefore little influence on the volume estimate and its accuracy. The largest craters seen on Lutetia have a diameter of about 20 km and a depth of about 2–3 km (see Fig. 4, and Marchi et al. 2011; Vincent et al. 2011), corresponding to the typical accuracy on elevation, and are therefore already included in the uncertainty envelop around the KOALA shape model.

From this detailed comparison of OSIRIS frames with KOALA predictions, we assert that the KOALA model performed extraordinarily well, especially given two limiting factors related to the observing geometries of the ground-based observations. First, for the imaging observations, Lutetia had an angular diameter of about 0.1″, close to the angular resolution for which we currently can extract useful shape information from ground-based telescopes with AO. Second, for the oppositions in 2007 and 2008, Lutetia was positioned at diametrically opposite apparent ecliptic coordinates from Earth, and because of the high obliquity, we observed Lutetia close to North-pole-on and then close to South-pole-on, and we were not able to achieve a good equatorial view, resulting in a poorly determined c-axis (Drummond et al. 2010; Carry et al. 2010b). We expect to improve that in upcoming observations.

We have determined the difference between the KOALA shape model and the *real* topography of Lutetia to be 2 km, on average. Considering Lutetia's volume-equivalent diameter (98 km, see Table 1), this translates into a relative precision on the radii of about 5%. We can therefore expect a conservative upper limit of 15% for the accuracy that can be achieved on volume estimates made by KOALA (including possible systematic effects), although it appears that the measured uncertainty (Fig. 6) is closer to 5%. These estimates of the accuracy achievable with KOALA are close to our previously

[11] Although the model does not show round, crater-like, features, KOALA allows modeling of concavities, that can be either large impact craters.

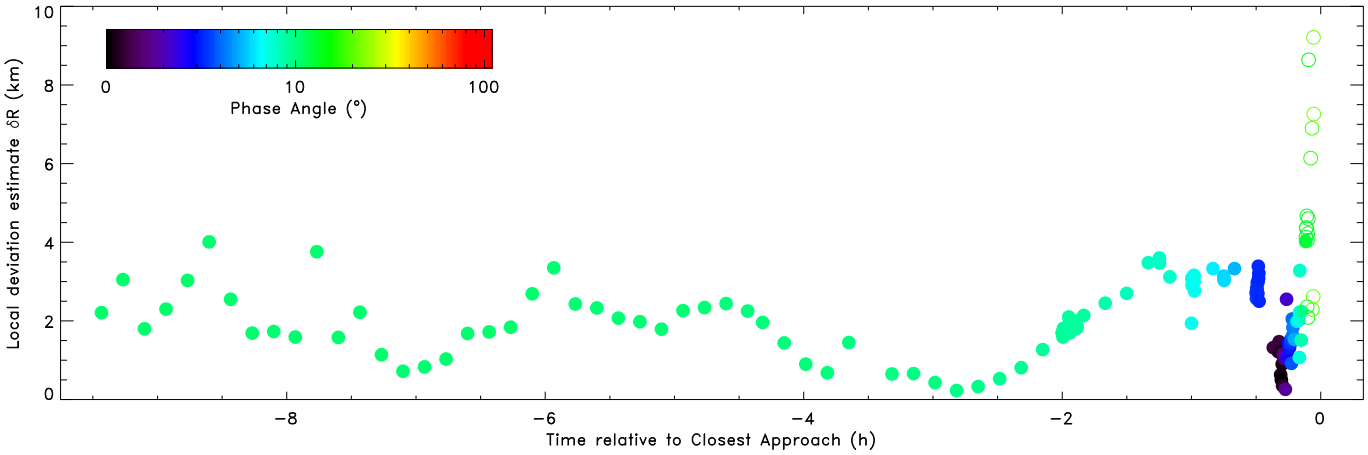

Figure 7: Estimate of the local deviation (δR) between the profiles of Lutetia extracted from the OSIRIS images and the prediction from the KOALA model (Carry et al. 2010b). The symbols are color-coded as a function of the phase angle. Filled symbols correspond to images where the phase angle was smaller than 10° (see text).

estimated uncertainty: Although formal uncertainties for our shape-fitting algorithms are closer to 1 or 2 km, we had estimated that our size measurements were affected by systematic errors at the level of 1–3% (from simulations and observations of Saturn's moons, see Carry 2009; Drummond et al. 2009).

p_V	Γ (SI)	References
assumed	20	Gulkis et al. (2011)
0.185 ± 0.005	5	O'Rourke et al. (2011)
0.19 ± 0.01	< 40	This work

Table 2: Albedo (p_V), and thermal inertia (Γ, in SI units: $\mathrm{J\,m^{-2}\,s^{-0.5}\,K^{-1}}$) derived using MIRO on-board Rosetta (Gulkis et al. 2011), ground-based data in combination with the shape model derived from Rosetta flyby (O'Rourke et al. 2011), and ground-based data in combination with the KOALA shape model (present study).

4. KOALA and thermal radiometry

As a supplementary investigation of the capabilities of KOALA for the study of a large sample of asteroids from ground-based observations, we analyze here the thermal properties of (21) Lutetia, using only ground-based information: the KOALA 3-D shape model (Drummond et al. 2010; Carry et al. 2010b), and 104 individual thermal measurements (O'Rourke et al. 2011, and reference therein), disregarding any information provided by the flyby of the asteroid by Rosetta. We then compare our results with those derived from the thermal infrared observations acquired by the MIRO instrument during Rosetta flyby (Gulkis et al. 2011). We also comment on the results obtained by O'Rourke et al. (2011) with the same data set, but using the 3-D shape model derived from Rosetta imaging (Sierks et al. 2011).

Many observations at thermal wavelengths are available: Lutetia was observed multiple times by several infrared survey missions, like IRAS in 1983, or Akari in 2006/2007, but it was also targeted by different observing campaigns from ground: IRTF, ESO-TIMMI2, and from space: Spitzer, Herschel (see O'Rourke et al. 2011, , for details on the observing circumstances).

First, we use the spin-vector coordinates provided by KOALA to determine the corresponding (lightcurve averaged) cross-sections for all observations that were used to derive the absolute magnitude of Lutetia: $\mathrm{H} = 7.25 \pm 0.01$ mag (Bowell et al. 1989; Belskaya et al. 2010). All observations were taken with sub-observer latitude between −70° and −85°, close to pole-on geometry, when the apparent average diameter of Lutetia was around 110–111 km (compared to its volume-equivalent diameter of 98 km, Sierks et al. 2011). The absolute magnitude of Lutetia was therefore slightly overestimated. We can still use it to determine the geometric visual albedo p_V via the relation: $\log p_V = 6.2559 - 2\log d - 0.4\mathrm{H}$ (Pravec and Harris 2007, and references therein), providing d is the average apparent diameter of Lutetia at the time of the observations. The combination of the KOALA shape model with the published absolute H magnitude leads to $p_V = 0.19 \pm 0.01$, in excellent agreement with the value derived during Rosetta flyby (0.19 ± 0.01, see Sierks et al. 2011).

Second, the knowledge of the 3-D shape allows us to correct this bias on the actual H magnitude of Lutetia: Published absolute magnitudes are typically derived from a limited number of latitudes of the sub-observer point, and represent therefore an approximation only to the *real* absolute magnitude. Using the knowledge of the 3-D shape model with an absolute size scale and the geometric albedo (see above), one can determine the proper geometry-independent H-mag. Indeed, the absolute magnitude is intended to be a general, object-related property, rather than an observed quantity valid only for certain geometries (Bowell et al. 1989). The H-mag for Lutetia, based on the KOALA shape model and the geometric visual albedo of $p_V = 0.19$, is therefore $\mathrm{H}_V = 7.42 \pm 0.03$.

We use this refined H-mag to proceed with radiometric analysis via a TPM code (Lagerros 1996, 1997, see Section 1.3).

This model considers a 1-D heat conduction into the surface, based on realistic surface conditions of illumination provided by the KOALA shape model (see O'Rourke et al. 2011, for details on such computations). As a complementary check of the techniques, we first determine the radiometric size and geometric albedo of Lutetia, regardless of the size information provided by the KOALA shape model (following the method by Müller et al. 2011). The calculation is based on the general thermal properties derived for large main-belt asteroids (Müller and Lagerros 2002), a wavelength-dependent emissivity model, a default thermal inertia Γ of 15 J m^{-2} s$^{-0.5}$ K^{-1}, and a default roughness implementation with 60% of the surface covered by craters and an RMS of the surface slopes of 0.7 (see, *e.g.*, Lagerros 1996, 1997, for definitions of these quantities). This leads to a radiometric volume-equivalent diameter (based on a dimensionless version of the KOALA 3-D shape model) of 99.8 ± 4.6 km and a geometric albedo p_V of 0.198 ± 0.017 (weighted mean values and standard deviations from the analysis of the 104 individual thermal measurements). These values are in agreement with the pre-flyby estimates (diameter of 98.3 ± 5.9 km and geometric albedo p_V of 0.208 ± 0.025) by Mueller et al. (2006), using the lightcurve inversion model by Torppa et al. (2003). This demonstrates the value of combining thermal data with spin and 3-D shape models to derive accurately the diameters and albedos of asteroids.

Finally, we constrain the thermal inertia of Lutetia by comparing the TPM predictions (using the KOALA 3-D shape model, including its size estimate) for a range of thermal inertias with the 104 observed thermal measurements. This allows us to find the most probable thermal inertia to explain all data simultaneously, *i.e.*, to match the before/after opposition observations as well as the observations taken at the short-wavelength Wien part of the spectral energy distribution (SED) and the long-wavelength Rayleigh-Jeans part of the SED. Thermal data also cover the entire rotation of Lutetia and a significant range of sub-Earth latitudes (see the listing of observations in O'Rourke et al. 2011). Thermal inertias in the range 5–40 J m^{-2} s$^{-0.5}$ K^{-1} produce the lowest χ^2-values (see Fig. 8), indicating the presence of fine-grained regolith (Brown and Matson 1987). These values are in agreement with the values measured by Rosetta (< 20 J m^{-2} s$^{-0.5}$ K^{-1}, see Gulkis et al. 2011). The χ^2-analysis also shows that one has to add substantial roughness on the surface to explain the thermal measurements. The KOALA 3-D shape model without any small-scale roughness cannot provide acceptable χ^2-values.

The prediction made using the combination of the KOALA and TPM models provides a good fit to all 104 measurements of Lutetia in the thermal infrared. There is a discrepancy, however, for a given observing geometry that could be solved by the addition of a plateau/hill to the 3-D shape model, whose size remains within the quoted 3-D shape uncertainty as discussed by O'Rourke et al. (2011).

From this detailed comparison of ground-based with flyby results, KOALA has been shown to be a powerful technique for the study of asteroids from the ground, not only for size/shape/spin, but now also for thermal properties. The validated (see Section 3) 3-D shape models, determined using KOALA, allow the study of the surface properties (*e.g.*, albedo, thermal inertia) in great detail, and the results are consistent with those derived from the flyby.

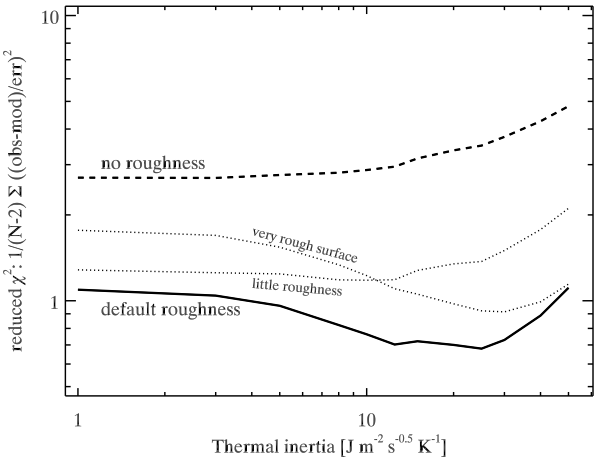

Figure 8: Thermal inertia determination using the KOALA shape model and ground-based observations. We use four values of surface roughness (default roughness means 60% of the surface is covered by craters and the RMS of the surface slopes is 0.7; see detail in O'Rourke et al. 2011) for thermal inertia ranging from very low to moderate (1–100 J m^{-2} s$^{-0.5}$ K^{-1}).

5. Concluding remarks: the future of KOALA

The flyby of (21) Lutetia by ESA Rosetta provided a spectacular demonstration of the capabilities of the KOALA algorithm. Spin-vector coordinates were found to be accurate within two degrees, 3-D shape modeling to better than 2 km (local topography), and dimensions to 2%. Volume estimates provided by KOALA are seen to be accurate to better than 10%. The thermal properties (albedo and thermal inertia) of Lutetia determined using a thermophysical model in conjunction with the KOALA shape model agree with the Rosetta-flyby-derived values, within the quoted uncertainties. These levels of accuracy on the spin and 3-D shape/size are typical for large main-belt asteroids, and not specific to Lutetia. Although it was extensively observed from the ground, being a spacecraft target, the number of lightcurves was similar to that of other large main-belt asteroids and the geometry of imaging observations was not particularly favorable (*i.e.*, mostly close to "pole-on").

This ability of KOALA to determine the volume of main-belt asteroids of size ~100 km with an accuracy of about 10% opens the possibility for study of a larger set of small bodies using Earth-based observations. For instance, it can be expected to help efforts to better understand the densities of asteroids belonging to different taxonomic classes (DeMeo et al. 2009). This will be assisted by mass estimates from about 150–200 asteroids that will be determined from gravitational deflections observed by the upcoming ESA Gaia astrometry mission (Mouret et al. 2007), and the ever-growing number of known binary asteroids. During the first stages of the encounter

of Rosetta with its main target, comet 67P/Churyumov-Gerasimenko in 2014, we also plan to use a KOALA-style analysis of the first, low-resolution, resolved images to quickly produce a shape/size model. This will support the mission science until a full high-resolution model can be derived.

The present implementation of KOALA allows the combined use of optical lightcurves (including sparse photometry), profiles from disk-resolved images, and chords from stellar occultations. We continue the development of KOALA toward the use of more data modes (*e.g.*, interferometry, thermal radiometry) to increase the number of possible targets, and to set better constraints on targets observable only with certain techniques. Using different wavelength ranges, in particular in the thermal infrared, opens the possibility of deriving additional physical properties, like albedo or thermal inertia. We also plan to incorporate additional cross-checks and constraints on the inversion, such as rigorous attention to differences in the spatial resolution of input images, to improve the confidence on the non-convex features and details.

Acknowledgments

We would like to thank the OSIRIS Team for use of the OSIRIS images. OSIRIS was built by a consortium of the Max-Planck-Institut für Sonnensystemforschung, Lindau, Germany, the Laboratoire d'Astrophysique de Marseille, France, the Centro Interdipartimentale Studi e Attivita' Spaziali, University of Padova, Italy, the Instituto de Astrofisica de Andalucia, Granada, Spain, the Research and Scientific Support Department of the European Space Agency (ESA/ESTEC), Noordwijk, The Netherlands, the Instituto Nacional de Tecnica Aerospacial, Madrid, Spain, the Institut für Datentechnik und Kommunikationsnetze der Technischen Universitat, Braunschweig and the Department of Astronomy and Space Physics of Uppsala University, Sweden. The support of the national funding agencies DLR, CNES, ASI, MEC, NASA, and SNSB is gratefully acknowledged. We thank the Rosetta Science Operations Center and the Rosetta Mission Operations Center for the successful flyby of (21) Lutetia. We would like to thank F. Preusker, S. Marchi, and J.-B. Vincent for providing their results ahead of publication. Herschel is an ESA space observatory with science instruments provided by European-led Principal Investigator consortia and with important participation from NASA. The thermal analysis is also based on observations collected at the European Southern Observatory, Chile: 79.C-0006. The KOALA shape model discussed here was based on imaging observations realized at the ESO Very Large Telescope (079.C-0493), and the W. M. Keck Observatory, which is operated as a scientific partnership among the California Institute of Technology, the University of California, and the National Aeronautics and Space Administration. The Observatory was made possible by the generous financial support of the W. M. Keck Foundation. We also thank our collaborators on Team Keck, the Keck science staff, for making possible some of these observations, and for observing time granted at Gemini Observatory under NOAO time allocation. This work was supported, in part, by the NASA Planetary Astronomy and NSF Planetary Astronomy Programs (Merline PI), and the work of J. Ďurech was supported by the grant GACR 209/10/0537 of the Czech Science Foundation. This research used Miriade VO tool (Berthier et al. 2008) developed at IMCCE, and NASA's Astrophysics Data System. Thanks to all the developers!

References

Baer, J., Chesley, S.R., Matson, R.D., 2011. Astrometric Masses of 26 Asteroids and Observations on Asteroid Porosity. Astronomical Journal 141, 143–155.

Behrend, R., Bernasconi, L., Roy, R., Klotz, A., Colas, F., Antonini, P., Aoun, R., Augustesen, K., Barbotin, E., Berger, N., Berrouachdi, H., Brochard, E., Cazenave, A., Cavadore, C., Coloma, J., Cotrez, V., Deconihout, S., Demeautis, C., Dorseuil, J., Dubos, G., Durkee, R., Frappa, E., Hormuth, F., Itkonen, T., Jacques, C., Kurtze, L., Laffont, A., Lavayssière, M., Lecacheux, J., Leroy, A., Manzini, F., Masi, G., Matter, D., Michelsen, R., Nomen, J., Oksanen, A., Pääkkönen, P., Peyrot, A., Pimentel, E., Pray, D.P., Rinner, C., Sanchez, S., Sonnenberg, K., Sposetti, S., Starkey, D., Stoss, R., Teng, J.P., Vignand, M., Waelchli, N., 2006. Four new binary minor planets: (854) Frostia, (1089) Tama, (1313) Berna, (4492) Debussy. Astronomy and Astrophysics 446, 1177–1184.

Belskaya, I.N., Fornasier, S., Krugly, Y.N., Shevchenko, V.G., Gaftonyuk, N.M., Barucci, M.A., Fulchignoni, M., Gil-Hutton, R.G., 2010. Puzzling asteroid 21 Lutetia: our knowledge prior to the Rosetta fly-by. Astronomy and Astrophysics 515, A29.

Berthier, J., Hestroffer, D., Carry, B., Ďurech, J., Tanga, P., Delbo, M., Vachier, F., 2008. A Service of Position and Physical Ephemerides Computation Dedicated to the Small Bodies of the Solar System. LPI Contributions 1405, 8374.

Binzel, R.P., Gaffey, M.J., Thomas, P.C., Zellner, B.H., Storrs, A.D., Wells, E.N., 1997. Geologic Mapping of Vesta from 1994 Hubble Space Telescope Images. Icarus 128, 95–103.

Bowell, E., Hapke, B., Domingue, D., Lumme, K., Peltoniemi, J., Harris, A.W., 1989. Application of photometric models to asteroids. Asteroids II , 524–556.

Britt, D.T., Yeomans, D.K., Housen, K.R., Consolmagno, G.J., 2002. Asteroid Density, Porosity, and Structure. Asteroids III , 485–500.

Brown, R.H., Matson, D.L., 1987. Thermal effects of insolation propagation into the regoliths of airless bodies. Icarus 72, 84–94.

Busch, M.W., 2009. ALMA and asteroid science. Icarus 200, 347–349.

Carry, B., 2009. Asteroids physical properties from high angular-resolution imaging. Ph.D. thesis. Observatoire de Paris.

Carry, B., Dumas, C., Fulchignoni, M., Merline, W.J., Berthier, J., Hestroffer, D., Fusco, T., Tamblyn, P., 2008. Near-Infrared Mapping and Physical Properties of the Dwarf-Planet Ceres. Astronomy and Astrophysics 478, 235–244.

Carry, B., Dumas, C., Kaasalainen, M., Berthier, J., Merline, W.J., Erard, S., Conrad, A.R., Drummond, J.D., Hestroffer, D., Fulchignoni, M., Fusco, T., 2010a. Physical properties of (2) Pallas. Icarus 205, 460–472.

Carry, B., Kaasalainen, M., Leyrat, C., Merline, W.J., Drummond, J.D., Conrad, A.R., Weaver, H.A., Tamblyn, P.M., Chapman, C.R., Dumas, C., Colas, F., Christou, J.C., Dotto, E., Perna, D., Fornasier, S., Bernasconi, L., Behrend, R., Vachier, F., Kryszczynska, A., Polinska, M., Fulchignoni, M., Roy, R., Naves, R., Poncy, R., Wiggins, P., 2010b. Physical properties of the ESA Rosetta target asteroid (21) Lutetia. II. Shape and flyby geometry. Astronomy and Astrophysics 523, A94.

Conrad, A.R., Dumas, C., Merline, W.J., Drummond, J.D., Campbell, R.D., Goodrich, R.W., Le Mignant, D., Chaffee, F.H., Fusco, T., Kwok, S.H., Knight, R.I., 2007. Direct measurement of the size, shape, and pole of 511 Davida with Keck AO in a single night. Icarus 191, 616–627.

Delbo, M., Dell'Oro, A., Harris, A.W., Mottola, S., Mueller, M., 2007. Thermal inertia of near-Earth asteroids and implications for the magnitude of the Yarkovsky effect. Icarus 190, 236–249.

Delbo, M., Gai, M., Lattanzi, M.G., Ligori, S., Loreggia, D., Saba, L., Cellino, A., Gandolfi, D., Licchelli, D., Blanco, C., Cigna, M., Wittkowski, M., 2006. MIDI observations of 1459 Magnya: First attempt of interferometric observations of asteroids with the VLTI. Icarus 181, 618–622.

Delbo, M., Ligori, S., Matter, A., Cellino, A., Berthier, J., 2009. First VLTI-MIDI Direct Determinations of Asteroid Sizes. Astrophysical Journal 694, 1228–1236.

Delbo, M., Tanga, P., 2009. Thermal inertia of main belt asteroids smaller than 100 km from IRAS data. Planetary and Space Science 57, 259–265.

DeMeo, F.E., Binzel, R.P., Slivan, S.M., Bus, S.J., 2009. An extension of the Bus asteroid taxonomy into the near-infrared. Icarus 202, 160–180.

Drummond, J.D., Christou, J.C., 2008. Triaxial ellipsoid dimensions and rotational poles of seven asteroids from Lick Observatory adaptive optics images, and of Ceres. Icarus 197, 480–496.

Drummond, J.D., Christou, J.C., Nelson, J., 2009. Triaxial ellipsoid dimensions and poles of asteroids from AO observations at the Keck-II telescope. Icarus 202, 147–159.

Drummond, J.D., Cocke, W.J., 1989. Triaxial ellipsoid dimensions and rotational pole of 2 Pallas from two stellar occultations. Icarus 78, 323–329.

Drummond, J.D., Conrad, A., Merline, W., Carry, B., 2009. The Dimensions and Pole of Asteroid (21) Lutetia from Adaptive Optics Images, in: AAS/Division for Planetary Sciences Meeting Abstracts #41, p. 59.07.

Drummond, J.D., Conrad, A., Merline, W.J., Carry, B., Chapman, C.R., Weaver, H.A., Tamblyn, P.M., Christou, J.C., Dumas, C., 2010. Physical properties of the ESA Rosetta target asteroid (21) Lutetia. I. The triaxial ellipsoid dimensions, rotational pole, and bulk density. Astronomy and Astrophysics 523, A93.

Drummond, J.D., Fugate, R.Q., Christou, J.C., Hege, E.K., 1998. Full Adaptive Optics Images of Asteroids Ceres and Vesta; Rotational Poles and Triaxial Ellipsoid Dimensions. Icarus 132, 80–99.

Dunham, D.W., Dunham, J.B., Binzel, R.P., Evans, D.S., Freuh, M., Henry, G.W., A'Hearn, M.F., Schnurr, R.G., Betts, R., Haynes, H., Orcutt, R., Bowell, E., Wasserman, L.H., Nye, R.A., Giclas, H.L., Chapman, C.R., Dietz, R.D., Moncivais, C., Douglas, W.T., Parker, D.C., Beish, J.D., Martin, J.O., Monger, D.R., Hubbard, W.B., Reitsema, H.J., Klemola, A.R., Lee, P.D., McNamara, B.R., Maley, P.D., Manly, P., Markworth, N.L., Nolthenius, R., Oswalt, T.D., Smith, J.A., Strother, E.F., Povenmire, H.R., Purrington, R.D., Trenary, C., Schneider, G.H., Schuster, W.J., Moreno, M.A., Guichard, J., Sanchez, G.R., Taylor, G.E., Upgren, A.R., von Flandern, T.C., 1990. The size and shape of (2) Pallas from the 1983 occultation of 1 Vulpeculae. Astronomical Journal 99, 1636–1662.

Ďurech, J., Grav, T., Jedicke, R., Denneau, L., Kaasalainen, M., 2005. Asteroid Models from the Pan-STARRS Photometry. Earth Moon and Planets 97, 179–187.

Ďurech, J., Kaasalainen, M., Herald, D., Dunham, D., Timerson, B., Hanuš, J., Frappa, E., Talbot, J., Hayamizu, T., Warner, B.D., Pilcher, F., Galád, A., 2011. Combining asteroid models derived by lightcurve inversion with asteroidal occultation silhouettes. Icarus 214, 652–670.

Ďurech, J., Kaasalainen, M., Marciniak, A., Allen, W.H., Behrend, R., Bembrick, C., Bennett, T., Bernasconi, L., Berthier, J., Bolt, G., Boroumand, S., Crespo da Silva, L.D., Crippa, R., Crow, M., Durkee, R., Dymock, R., Fagas, M., Fauerbach, M., Fauvaud, S., Frey, M., Gonçalves, R., Hirsch, R., Jardine, D., Kamiński, K., Koff, R., Kwiatkowski, T., López, A., Manzini, F., Michałowski, T., Pacheco, R., Pan, M., Pilcher, F., Poncy, R., Pray, D.P., Pych, W., Roy, R., Santacana, G., Slivan, S.M., Sposetti, S., Stephens, R., Warner, B.D., Wolf, M., 2007. Physical models of ten asteroids from an observers' collaboration network. Astronomy and Astrophysics 465, 331–337.

Ďurech, J., Sidorin, V., Kaasalainen, M., 2010. DAMIT: a database of asteroid models. Astronomy and Astrophysics 513, A46.

Elkins-Tanton, L.T., Weiss, B.P., Zuber, M.T., 2011. Chondrites as samples of differentiated planetesimals. Earth and Planetary Science Letters 305, 1–10.

Fujiwara, A., Kawaguchi, J., Yeomans, D.K., Abe, M., Mukai, T., Okada, T., Saito, J., Yano, H., Yoshikawa, M., Scheeres, D.J., Barnouin-Jha, O.S., Cheng, A.F., Demura, H., Gaskell, G.W., Hirata, N., Ikeda, H., Kominato, T., Miyamoto, H., Nakamura, R., Sasaki, S., Uesugi, K., 2006. The Rubble-Pile Asteroid Itokawa as Observed by Hayabusa. Science 312, 1330–1334.

Gaskell, R.W., Barnouin-Jha, O.S., Scheeres, D.J., Konopliv, A.S., Mukai, T., Abe, S., Saito, J., Ishiguro, M., Kubota, T., Hashimoto, T., Kawaguchi, J., Yoshikawa, M., Shirakawa, K., Kominato, T., Hirata, N., Demura, H., 2008. Characterizing and navigating small bodies with imaging data. Meteoritics and Planetary Science 43, 1049–1061.

Gulkis, S., Frerking, M., Crovisier, J., Beaudin, G., Hartogh, P., Encrenaz, P., Koch, T., Kahn, C., Salinas, Y., Nowicki, R., Irigoyen, R., Janssen, M., Stek, P., Hofstadter, M., Allen, M., Backus, C., Kamp, L., Jarchow, C., Steinmetz, E., Deschamps, A., Krieg, J., Gheudin, M., Bockelée-Morvan, D., Biver, N., Encrenaz, T., Despois, D., Ip, W.H., Lellouch, E., Mann, I., Muhleman, D., Rauer, H., Schloerb, P., Spilker, T., 2011. Continuum and Spectroscopic Observations of Asteroid (21) Lutetia at Millimeter and Submillimeter Wavelengths with the MIRO Instrument on the Rosetta Spacecraft. Planetary and Space Science same issue.

Hanuš, J., Ďurech, J., Brož, M., Warner, B.D., Pilcher, F., Stephens, R., Oey, J., Bernasconi, L., Casulli, S., Behrend, R., Polishook, D., Henych, T., Lehký, M., Yoshida, F., Ito, T., 2011. A study of asteroid pole-latitude distribution based on an extended set of shape models derived by the lightcurve inversion method. Astronomy and Astrophysics 530, A134.

Hestroffer, D., Tanga, P., Cellino, A., Guglielmetti, F., Lattanzi, M.G., di Martino, M., Zappalà, V., Berthier, J., 2002. Asteroids observations with the Hubble Space Telescope. I. Observing strategy, and data analysis and modeling process. Astronomy and Astrophysics 391, 1123–1132.

Hill, J.M., Green, R.F., Ashby, D.S., Brynnel, J.G., Cushing, N.J., Little, J., Slagle, J.H., Wagner, R.M., 2010. The Large Binocular Telescope. SPIE 7733.

Hilton, J.L., 2002. Asteroid Masses and Densities. Asteroids III , 103–112.

Housen, K.R., Holsapple, K.A., Voss, M.E., 1999. Compaction as the origin of the unusual craters on the asteroid Mathilde. Nature 402, 155–157.

Johansen, A., Lacerda, P., 2010. Prograde rotation of protoplanets by accretion of pebbles in a gaseous environment. Monthly Notices of the Royal Astronomical Society 404, 475–485.

Kaasalainen, M., 2004. Physical models of large number of asteroids from calibrated photometry sparse in time. Astronomy and Astrophysics 422, L39–L42.

Kaasalainen, M., 2011. Maximum compatibility estimates and shape reconstruction with boundary curves and volumes of generalized projections. Inverse Problems and Imaging 5, 37–57.

Kaasalainen, M., Lamberg, L., 2006. Inverse problems of generalized projection operators. Inverse Problems 22, 749–769.

Kaasalainen, M., Mottola, S., Fulchignoni, M., 2002a. Asteroid Models from Disk-integrated Data. Asteroids III , 139–150.

Kaasalainen, M., Torppa, J., 2001. Optimization Methods for Asteroid Lightcurve Inversion - I. Shape Determination. Icarus 153, 24–36.

Kaasalainen, M., Torppa, J., Muinonen, K., 2001. Optimization Methods for Asteroid Lightcurve Inversion - II. The Complete Inverse Problem. Icarus 153, 37–51.

Kaasalainen, M., Torppa, J., Piironen, J., 2002b. Models of Twenty Asteroids from Photometric Data. Icarus 159, 369–395.

Keller, H.U., Barbieri, C., Lamy, P.L., Rickman, H., Rodrigo, R., Wenzel, K.P., Sierks, H., A'Hearn, M.F., Angrilli, F., Angulo, M., Bailey, M.E., Barthol, P., Barucci, M.A., Bertaux, J.L., Bianchini, G., Boit, J.L., Brown, V., Burns, J.A., Büttner, I., Castro, J.M., Cremonese, G., Curdt, W., da Deppo, V., Debei, S., de Cecco, M., Dohlen, K., Fornasier, S., Fulle, M., Germerott, D., Gliem, F., Guizzo, G.P., Hviid, S.F., Ip, W.H., Jorda, L., Koschny, D., Kramm, J.R., Kührt, E., Küppers, M., Lara, L.M., Llebaria, A., López, A., López-Jimenez, A., López-Moreno, J., Meller, R., Michalik, H., Michelena, M.D., Müller, R., Naletto, G., Origné, A., Parzianello, G., Pertile, M., Quintana, C., Ragazzoni, R., Ramous, P., Reiche, K.U., Reina, M., Rodríguez, J., Rousset, G., Sabau, L., Sanz, A., Sivan, J.P., Stöckner, K., Tabero, J., Telljohann, U., Thomas, N., Timon, V., Tomasch, G., Wittrock, T., Zaccariotto, M., 2007. OSIRIS The Scientific Camera System Onboard Rosetta. Space Science Reviews 128, 433–506.

Lagerros, J.S.V., 1996. Thermal physics of asteroids. I. Effects of shape, heat conduction and beaming. Astronomy and Astrophysics 310, 1011–1020.

Lagerros, J.S.V., 1997. Thermal physics of asteroids. III. Irregular shapes and albedo variegations. Astronomy and Astrophysics 325, 1226–1236.

Lamy, P.L., Jorda, L., Fornasier, S., Groussin, O., Barucci, M.A., Carvano, J.M., Dotto, E., Fulchignoni, M., Toth, I., 2008a. Asteroid 2867 Steins. III. Spitzer Space Telescope observations, size determination, and thermal properties. Astronomy and Astrophysics 487, 1187–1193.

Lamy, P.L., Kaasalainen, M., Lowry, S.C., Weissman, P., Barucci, M.A., Carvano, J.M., Choi, Y., Colas, F., Faury, G., Fornasier, S., Groussin, O., Hicks, M.D., Jorda, L., Kryszczynska, A., Larson, S., Toth, I., Warner, B.D., 2008b. Asteroid 2867 Steins. II. Multi-telescope visible observations, shape reconstruction, and rotational state. Astronomy and Astrophysics 487, 1179–1185.

Lebofsky, L.A., Sykes, M.V., Tedesco, E.F., Veeder, G.J., Matson, D.L., Brown, R.H., Gradie, J.C., Feierberg, M.A., Rudy, R.J., 1986. A refined 'standard' thermal model for asteroids based on observations of 1 Ceres and 2 Pallas.

Icarus 68, 239–251.
Li, J., Kuchner, M.J., Allen, R.J., Sheppard, S.S., 2011. Measuring the sizes, shapes, surface features and rotations of Solar System objects with interferometry. Icarus 211, 1007–1021.
Li, J., McFadden, L.A., Thomas, P.C., Mutchler, M.J., Parker, J.W., Young, E.F., Russell, C.T., Sykes, M.V., Schmidt, B.E., 2010. Photometric mapping of Asteroid (4) Vesta's southern hemisphere with Hubble Space Telescope. Icarus 208, 238–251.
Li, J.Y., McFadden, L.A., Parker, J.W., Young, E.F., Stern, S.A., Thomas, P.C., Russell, C.T., Sykes, M.V., 2006. Photometric analysis of 1 Ceres and surface mapping from HST observations. Icarus 182, 143–160.
Mainzer, A., Bauer, J.M., Grav, T., Masiero, J., Cutri, R.M., Dailey, J., Eisenhardt, P., McMillan, R.S., Wright, E., Walker, R.G., Jedicke, R., Spahr, T., Tholen, D.J., Alles, R., Beck, R., Brandenburg, H., Conrow, T., Evans, T., Fowler, J., Jarrett, T., Marsh, K., Masci, F., McCallon, H., Wheelock, S., Wittman, M., Wyatt, P., DeBaun, E., Elliott, G., Elsbury, D., Gautier, T., Gomillion, S., Leisawitz, D., Maleszewski, C., Micheli, M., Wilkins, A., 2011. Preliminary Results from NEOWISE: An Enhancement to the Wide-field Infrared Survey Explorer for Solar System Science. Astrophysical Journal 731, 53–66.
Marchi, S., Massironi, M., Vincent, J., Morbidelli, A., Mottola, S., Marzari, F., Küppers, M., Besse, S., Thomas, N., Barbieri, C., Naletto, G., Sierks, H., 2011. The Cratering History of Asteroid (21) Lutetia. Planetary and Space Science same issue.
Matter, A., Delbo, M., Ligori, S., Crouzet, N., Tanga, P., 2011. Determination of physical properties of the asteroid (41) Daphne from interferometric observations in the thermal infrared. Icarus 215, 47–56.
Merline, W.J., Drummond, J.D., Conrad, A.R., Carry, B., Dumas, C., 2011. The Resolved Asteroid Program - I: (52) Europa. submitted to Icarus .
Merline, W.J., Weidenschilling, S.J., Durda, D.D., Margot, J.L., Pravec, P., Storrs, A.D., 2002. Asteroids Do Have Satellites. Asteroids III , 289–312.
Millis, R.L., Dunham, D.W., 1989. Precise measurement of asteroid sizes and shapes from occultations. Asteroids II , 148–170.
Moullet, A., Lellouch, E., Moreno, R., Gurwell, M., 2011. Physical studies of Centaurs and Trans-Neptunian Objects with the Atacama Large Millimeter Array. Icarus 213, 382–392.
Mouret, S., Hestroffer, D., Mignard, F., 2007. Asteroid masses and improvement with GAIA. Astronomy and Astrophysics 472, 1017–1027.
Mueller, M., Harris, A.W., Bus, S.J., Hora, J.L., Kassis, M., Adams, J.D., 2006. The size and albedo of Rosetta fly-by target 21 Lutetia from new IRTF measurements and thermal modeling. Astronomy and Astrophysics 447, 1153–1158.
Müller, T.G., Ďurech, J., Hasegawa, S., Abe, M., Kawakami, K., Kasuga, T., Kinoshita, D., Kuroda, D., Urakawa, S., Okumura, S., Sarugaku, Y., Miyasaka, S., Takagi, Y., Weissman, P.R., Choi, Y.J., Larson, S., Yanagisawa, K., Nagayama, S., 2011. Thermo-physical properties of 162173 (1999 JU3), a potential flyby and rendezvous target for interplanetary missions. Astronomy and Astrophysics 525, A145.
Müller, T.G., Lagerros, J.S.V., 2002. Asteroids as calibration standards in the thermal infrared for space observatories. Astronomy and Astrophysics 381, 324–339.
Müller, T.G., Sekiguchi, T., Kaasalainen, M., Abe, M., Hasegawa, S., 2005. Thermal infrared observations of the Hayabusa spacecraft target asteroid 25143 Itokawa. Astronomy and Astrophysics 443, 347–355.
O'Rourke, L., Müller, T.G., Valtchanov, I., Altieri, B., Gonzlez-Garcia, B., Bhattacharya, B., Carry, B., 2011. Thermal & Shape properties of Asteroid (21) Lutetia from Herschel Observations around the Rosetta Flyby. Planetary and Space Science same issue.
Ostro, S.J., 1989. Radar observations of asteroids. Asteroids II , 192–212.
Ostro, S.J., Benner, L.A.M., Magri, C., Giorgini, J.D., Rose, R., Jurgens, R.F., Yeomans, D.K., Hine, A.A., Nolan, M.C., Scheeres, D.J., Broschart, S.B., Kaasalainen, M., Margot, J., 2005. Radar observations of Itokawa in 2004 and improved shape estimation. Meteoritics and Planetary Science 40, 1563–1574.
Ostro, S.J., Hudson, R.S., Benner, L.A.M., Giorgini, J.D., Magri, C., Margot, J.L., Nolan, M.C., 2002. Asteroid Radar Astronomy. Asteroids III , 151–168.
Ostro, S.J., Margot, J.L., Benner, L.A.M., Giorgini, J.D., Scheeres, D.J., Fahnestock, E.G., Broschart, S.B., Bellerose, J., Nolan, M.C., Magri, C., Pravec, P., Scheirich, P., Rose, R., Jurgens, R.F., De Jong, E.M., Suzuki, S., 2006. Radar Imaging of Binary Near-Earth Asteroid (66391) 1999 KW4. Science 314, 1276–1280.
Parker, J.W., McFadden, L.A., Russell, C.T., Stern, S.A., Sykes, M.V., Thomas, P.C., Young, E.F., 2006. Ceres: High-resolution imaging with HST and the determination of physical properties. Advances in Space Research 38, 2039–2042.
Parker, J.W., Stern, S.A., Thomas, P.C., Festou, M.C., Merline, W.J., Young, E.F., Binzel, R.P., Lebofsky, L.A., 2002. Analysis of the First Disk-resolved Images of Ceres from Ultraviolet Observations with the Hubble Space Telescope. The Astronomical Journal 123, 549–557.
Pravec, P., Harris, A.W., 2007. Binary asteroid population. 1. Angular momentum content. Icarus 190, 250–259.
Preusker, F., Scholten, F., Knollenberg, J., Khrt, E., Matz, K.D., Mottola, S., Roatsch, T., Thomas, N., 2011. The Northern hemisphere of asteroid 21 Lutetia Topography and orthoimages from Rosetta OSIRIS NAC image data. Planetary and Space Science same issue.
Roques, F., Boissel, Y., Doressoundiram, A., Sicardy, B., Widemann, T., 2009. Exploration of the Outer Solar System by Stellar Occultations. Earth Moon and Planets 105, 201–208.
Ryan, E.L., Woodward, C.E., 2010. Rectified Asteroid Albedos and Diameters from IRAS and MSX Photometry Catalogs. Astronomical Journal 140, 933–943. 1006.4362.
Saint-Pé, O., Combes, M., Rigaut, F., 1993a. Ceres surface properties by high-resolution imaging from earth. Icarus 105, 271–281.
Saint-Pé, O., Combes, M., Rigaut, F., Tomasko, M., Fulchignoni, M., 1993b. Demonstration of adaptive optics for resolved imagery of solar system objects - Preliminary results on Pallas and Titan. Icarus 105, 263–270.
Schmidt, B.E., Thomas, P.C., Bauer, J.M., Li, J., McFadden, L.A., Mutchler, M.J., Radcliffe, S.C., Rivkin, A.S., Russell, C.T., Parker, J.W., Stern, S.A., 2009. The Shape and Surface Variation of 2 Pallas from the Hubble Space Telescope. Science 326, 275–278.
Sicardy, B., Widemann, T., Lellouch, E., Veillet, C., Cuillandre, J., Colas, F., Roques, F., Beisker, W., Kretlow, M., Lagrange, A., Gendron, E., Lacombe, F., Lecacheux, J., Birnbaum, C., Fienga, A., Leyrat, C., Maury, A., Raynaud, E., Renner, S., Schultheis, M., Brooks, K., Delsanti, A., Hainaut, O.R., Gilmozzi, R., Lidman, C., Spyromilio, J., Rapaport, M., Rosenzweig, P., Naranjo, O., Porras, L., Díaz, F., Calderón, H., Carrillo, S., Carvajal, A., Recalde, E., Cavero, L.G., Montalvo, C., Barría, D., Campos, R., Duffard, R., Levato, H., 2003. Large changes in Pluto's atmosphere as revealed by recent stellar occultations. Nature 424, 168–170.
Sierks, H., Lamy, P., Barbieri, C., Koschny, D., Rickman, H., Rodrigo, R., A'Hearn, M.F., Angrilli, F., Barucci, A., Bertaux, J.L., Bertini, I., Besse, S., Carry, B., Cremonese, G., Da Deppo, V., Davidsson, B., Debei, S., De Cecco, M., De Leon, J., Ferri, F., Fornasier, S., Fulle, M., Hviid, S.F., Gaskell, G.W., Groussin, O., Gutierrez, P.J., Jorda, L., Kaasalainen, M., Keller, H.U., Knollenberg, J., Kramm, J.R., Kührt, E., Küppers, M., Lara, L.M., Lazzarin, M., Leyrat, C., Lopez Moreno, J.L., Magrin, S., Marchi, S., Marzari, F., Massironi, M., Michalik, H., Moissl, R., Naletto, G., Preusker, F., Sabau, L., Sabolo, W., Scholten, F., Snodgrass, C., Thomas, N., Tubiana, C., Vernazza, P., Vincent, J.B., Wenzel, K.P., Andert, T., Pätzold, M., Weiss, B.P., 2011. Images of asteroid (21) Lutetia: A remnant planetesimal from the early Solar System. Science 334, 487–490.
Slivan, S.M., Binzel, R.P., Crespo da Silva, L.D., Kaasalainen, M., Lyndaker, M.M., Krčo, M., 2003. Spin vectors in the Koronis family: comprehensive results from two independent analyses of 213 rotation lightcurves. Icarus 162, 285–307.
Tanga, P., Delbo, M., 2007. Asteroid occultations today and tomorrow: toward the GAIA era. Astronomy and Astrophysics 474, 1015–1022.
Tanga, P., Hestroffer, D., Berthier, J., Cellino, A., Lattanzi, M.G., di Martino, M., Zappalá, V., 2001. HST/FGS Observations of the Asteroid (216) Kleopatra. Icarus 153, 451–454.
Tanga, P., Hestroffer, D., Cellino, A., Lattanzi, M.G., di Martino, M., Zappalà, V., 2003. Asteroid observations with the Hubble Space Telescope. II. Duplicity search and size measurements for 6 asteroids. Astronomy and Astrophysics 401, 733–741.
Tedesco, E.F., Noah, P.V., Noah, M.C., Price, S.D., 2002. The Supplemental IRAS Minor Planet Survey. Astronomical Journal 123, 1056–1085.
Thomas, N., Barbieri, C., Keller, H.U., Lamy, P., Rickman, H., Rodrigo, R., Sierks, H., Wenzel, K.P., Cremonese, G., Jorda, L., Marzari, F., Massironi, M., Preusker, F., Scholten, F., Stephan, K., Barucci, A., Besse, S., Fornasier, S., Groussin, O., Hviid, S.F., Koschny, D., Kührt, E., Küppers, M., Marchi, S., Martelleto, E., Moissl, R., Snodgrass, C., Tubiana, C., Vincent, J.B.,

2011. The geomorphology of 21 Lutetia: Results from the OSIRIS imaging system onboard ESAs Rosetta spacecraft. Planetary and Space Science same issue.

Thomas, P.C., Binzel, R.P., Gaffey, M.J., Storrs, A.D., Wells, E.N., Zellner, B.H., 1997a. Impact excavation on asteroid 4 Vesta: Hubble Space Telescope results. Science 277, 1492–1495.

Thomas, P.C., Binzel, R.P., Gaffey, M.J., Zellner, B.H., Storrs, A.D., Wells, E.N., 1997b. Vesta: Spin Pole, Size, and Shape from HST Images. Icarus 128, 88–94.

Thomas, P.C., Parker, J.W., McFadden, L.A., Russell, C.T., Stern, S.A., Sykes, M.V., Young, E.F., 2005. Differentiation of the asteroid Ceres as revealed by its shape. Nature 437, 224–226.

Torppa, J., Kaasalainen, M., Michalowski, T., Kwiatkowski, T., Kryszczyńska, A., Denchev, P., Kowalski, R., 2003. Shapes and rotational properties of thirty asteroids from photometric data. Icarus 164, 346–383.

Veverka, J., Thomas, P.C., Harch, A., Clark, B.E., Bell, J.F., Carcich, B., Joseph, J., Chapman, C.R., Merline, W.J., Robinson, M.S., Malin, M., McFadden, L.A., Murchie, S.L., Hawkins, S.E., Faquhar, R., Izenberg, N., Cheng, A.F., 1997. NEARs Flyby of 253 Mathilde: Images of a C Asteroid. Science 278, 2109–2114.

Vincent, J.B., Besse, S., Marchi, S., Sierks, H., Massironi, M., the OSIRIS Team, 2011. Physical properties of craters on asteroid (21) Lutetia. Planetary and Space Science same issue.

Walsh, K.J., Richardson, D.C., Michel, P., 2008. Rotational breakup as the origin of small binary asteroids. Nature 454, 188–191.

Warner, B.D., Harris, A.W., Pravec, P., 2009. The asteroid lightcurve database. Icarus 202, 134–146.